Chapter 12
Kinetic Assembly of Porous Coordination Networks Leads to Trapping Unstable Elemental Allotropes

Hiroyoshi Ohtsu, Pavel M. Usov, and Masaki Kawano

Abstract Kinetic assembly is an important method for obtaining desired materials in chemical synthesis and material sciences. However, the application of this strategy to porous coordination networks has been limited. We highlight the kinetic assembly of porous coordination networks, which promote the production of interactive pore sites. These sites can activate or stabilize different guest molecules. The properties of interactive pores are exemplified by iodine chemisorption and small sulfur encapsulation. Using the interactive feature of these pores, we were able to trap small sulfur allotropes, such as S_2, cyclo-S_3, bent-S_3, and S_6, demonstrating their importance for the stabilization of unusual elemental species. Furthermore, several reactive elemental allotropes could also be incorporated into the interactive pores. Herein, we address the important aspects of creating interactive pore sites by kinetic assembly of porous coordination networks and present detailed case-by-case studies of small allotrope encapsulation.

Keywords Porous coordination network · Kinetic assembly · Unstable small sulfur species · Elemental allotropes

12.1 Introduction

12.1.1 Scope of the Book Chapter

The kinetic assembly method for the coordination network formation is introduced in this chapter. This method is not common in coordination network chemistry, despite it having a great capacity to create functional materials. Furthermore, the kinetically assembled networks enabled us to successfully trap and visualize unstable elemental allotropes.

H. Ohtsu · P. M. Usov · M. Kawano (✉)
Tokyo Institute of Technology, Tokyo, Japan
e-mail: mkawano@chem.titech.ac.jp

© Springer Nature Singapore Pte Ltd. 2020

M. Sakamoto and H. Uekusa (eds.), *Advances in Organic Crystal Chemistry*,
https://doi.org/10.1007/978-981-15-5085-0_12

12.1.2 Kinetically Controlled Network Formation

Kinetic control of chemical reactions is a critical tool to produce desired products in chemical synthesis and material sciences. Diamond, one of the carbon allotropes, is less stable than graphite, which means that it is a metastable state. However, because of the large activation energy required to transform diamond to graphite, it remains as a stable crystalline solid under ambient conditions. This is a typical example of kinetically stabilized phase found in nature. Many researchers have used kinetic control to direct reactions along alternative pathways to produce desired products. In particular, in organic syntheses, kinetic control (or resolution) is often crucial to selectively obtain only one specific molecule and limit side reactions [1]. Biological systems use kinetically trapped states in living cells to sustain their function. For example, the protein folding can be finely tuned through kinetically guided assembly [2, 3]. Furthermore, the synthesis of inorganic materials, such as zeolites, is typically carried out under kinetic control [4, 5].

In addition, kinetic assembly was used to change the morphology of materials to create functional nanostructures via weak intermolecular interactions [6–8]. For example, the complexation of perylene tetracarboxylate (PTC) with Ni^{2+} displays selective kinetic/thermodynamic assembly depending on reaction temperatures. The coordinating amphiphile, PTC, has a planar conjugated skeleton. At temperatures below 25 °C, the intermolecular coordination between PTC and Ni^{2+} extends the coordinating system along the long axis of PTC, resulting in a microbelt structure several micrometers in length. However, PTC in this coordination mode is not planar, therefore, the system cannot minimize its energy via π–π stacking, indicating that it is a kinetic product. In contrast, at temperatures above 60 °C, PTC–Ni undergoes intramolecular coordination where the ligand adopts a planar conformation, facilitating π–π stacking. Consequently, it can be concluded that PTC–Ni self-assembles into much shorter nanorods under thermodynamic conditions. The two morphologies exhibit vastly differing electronic properties. The kinetically assembled microbelts have excellent electronic conductivity [6]. In another example, kinetic control was used to obtain various metal phenolic network (MPN) films. For this purpose, temporal and spatial control of MPN growth by promoting self-correction of the coordinating building blocks through oxidation-mediated network assembly was utilized [7]. The formation and growth mechanisms were investigated and used to engineer films with microporous structures and continuous gradients. These results show that morphological structure control by kinetic assembly is a promising strategy for producing functional materials.

However, for coordination networks, also known as coordination polymers (CPs) or metal–organic frameworks (MOFs), kinetic control has not been commonly employed in their synthesis [9–23]. Normally, the networks are synthesized under harsh conditions that lead to thermodynamically stable crystalline structures. For example, solvothermal reactions, which are carried out in a solvent close to or above its boiling point, and often under autogenous pressure, produce network single crystals. Some of the most thermally stable materials reported, such as MOF-5, HKUST-1,

MIL-101, and UiO-66 [24] are obtained using this technique. These types of synthesis are classified as thermodynamic assembly because the final product, including the solvent and adducts, represents a global energy minimum on the reaction coordinate landscape. In contrast, kinetic assembly traps metastable states during crystallization before equilibrium is reached, which requires much faster formation rates. The kinetic products tend to form polycrystalline powders rather than single crystals suitable for single-crystal structure analysis. As a result, the kinetic network formation has not been widely explored because of the difficulty of ab initio structure determination of crystalline powders by X-ray diffraction.

There are several examples of the kinetic assembly of coordination networks [4, 25–31]. The Cd-based network, [Cd(bpy)(bdc)] (bpy = 4,4′-bipyridine, bdc = 1,4-benzenedicarboxylate) can be generated as a single non-interpenetrating net by kinetic control at low temperature or high concentration. Whereas an interpenetrating network is obtained under thermodynamic control at high temperature or low concentration [25]. The interpenetration creates more stable structures relative to their non-interpenetrating analogues due to increase of crystal density and reduction of void space. Therefore, an increase in the degree of interpenetration tends to stabilize network structures. The consequence of this behavior is the increase of the accessible pore space inside the kinetically assembled networks, which could be beneficial for several applications, such as gas storage and separation. However, the fine balance between stability and porosity needs to be carefully controlled to achieve the desired material. Recently, this concept was applied to the synthesis of Fe-bpdc (bipy = biphenyl-4,4′-dicarboxylate) MOFs [26].

Other methods for the control of reaction pathways during coordination polymer synthesis have been reported. The most common approach is simply changing the reaction temperature to produce different network polymorphs. Cheetham et al. reported that they could obtain five structures from an identical starting mixture of $Co(OH)_3$ and succinic acid by running the reaction at five different temperatures [32]. In another example, a one-dimensional (1D) coordination polymer was formed by kinetical trapping of the reaction mixture of ZnI_2 and pyrimidine [33]. These results highlight the tendency of kinetically assembled networks to contain larger internal voids and exhibit lower density [34–39].

Another important feature of kinetic assembly is the creation of interactive sites within the structure [40, 41]. Since this process halts the network formation before it can reach a thermodynamic equilibrium by trapping metastable intermediate states, the resultant structures could contain “under-reacted” sites. In contrast, the thermodynamic structures typically have minimal latent reactivity and therefore are comparatively inert.

Figure 12.1 shows the schematic difference between thermodynamic and kinetic assemblies. In the former situation, the coordinating groups on the linkers and open sites around the coordination sphere of metal centers are fully paired up. Whereas in the latter case, some connecting sites remain unoccupied, resulting in pore environments that can interact with guest molecules.

In the following section, we will describe how interactive pores can be obtained by kinetic assembly and discuss their applications. In particular, we will demonstrate the

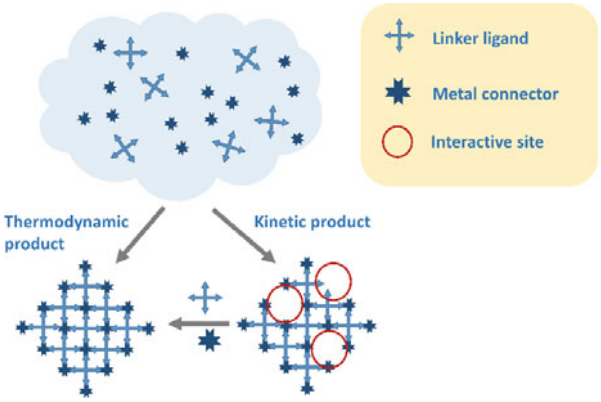

Fig. 12.1 Example of kinetic and thermodynamic assemblies of coordination networks. Reproduced by permission of The Royal Society of Chemistry

use of interactive sites inside networks to stabilize and crystallographically visualize highly reactive elemental allotropes.

12.1.3 Kinetic Assembly of Coordination Networks Using Zn Units

Kinetic assembly facilitates properties that are useful for creating functional materials, such as interactive pore sites and open non-interpenetrating structures. We developed the rapid synthetic method for kinetically controlled assembly of coordination networks [42]. This approach involves simple mixing of metal precursors (nodes) and organic ligands (linkers) in solution, which results in instantaneous reaction and network crystallization. In our first attempts, we used 2,4,6-tri(4-pyridyl)-1,3,5-triazine (TPT; Fig. 12.2) as a tridentate ligand.

When a nitrobenzene/methanol solution containing TPT was mixed with a methanol solution of $ZnBr_2$, a crystalline powder composed of micrometer-sized (<10 μm) uniform particles precipitated instantly (~30 s). The PXRD pattern of the crystalline powder indicated that the formation of a coordination network had occurred. The crystal structure was determined by ab initio PXRD analysis, which determined that it had the molecular formula of $[(ZnBr_2)_3(TPT)_2]$ and was isostructural with a related ZnI-based network, $[(ZnI_2)_3(TPT)_2]$. The structure of the iodide analogue contained a large flexible channel capable of reversible guest uptake and release in the crystalline state (Fig. 12.2) [42].

The structure of the kinetically assembled network was different from a polymorph formed under thermodynamic control. The thermodynamic network obtained by the layer diffusion method, $[(ZnBr_2)_3(TPT)_2]$, had 1D channels formed by π–π stacking of TPT (Fig. 12.2, left). This material exhibited a greater number of

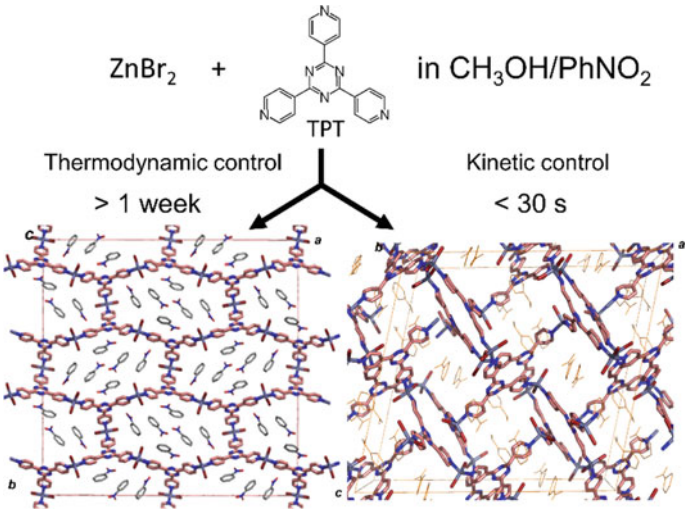

Fig. 12.2 Kinetic and thermodynamic control of network formation from $ZnBr_2$ and TPT. Reproduced by permission of The Royal Society of Chemistry

intramolecular interactions in its structure than the kinetic analogue. The thermodynamic/kinetic product assignment of these structures is consistent with their synthetic procedures—rapid crystallization resulted in a kinetic material, whereas the slower thermally equilibrated reaction gave the thermodynamic network. Moreover, the rapidly precipitated product can be converted to the more stable network by heating the crystalline powder, as determined by PXRD and differential scanning calorimetry (DSC), which provides additional evidence for the relative stabilities of the two materials. The PXRD measurements showed that the phase transformation of kinetically assembled network to the thermodynamic analogue occurred at 553 K. The DSC curve of the kinetical product showed an exothermic peak (40.10 kJ/mol) centered at 553 K, which was about three times larger than that for the other network. These results indicate that the rapidly synthesized network is a metastable state. Therefore, this type of synthetic method is convenient for producing kinetic phases. However, because the resultant products are often isolated as microcrystalline powders, ab initio PXRD analysis is the most suitable structure determination method for kinetically assembled coordination networks.

The rapid precipitation method was also applied with ZnI_2 metal connector. When a nitrobenzene/methanol solution of TPT was mixed with a methanol solution of ZnI_2, a crystalline powder quickly appeared. The crystal structure determined by ab initio PXPD analysis showed that it consisted of doubly interpenetrating 10,3-nets with the formula $[(ZnI_2)_3(TPT)_2]$ [43, 44]. In the network, the Zn atom is coordinated by two nitrogen atoms from TPT linkers and two iodides. This type of structure has been reported previously [42].

The interpenetrating network obtained under kinetic control, $[(ZnI_2)_3(TPT)_2]$, exhibited an unusual crystalline-to-amorphous-to-amorphous-to-crystalline (CAAC)

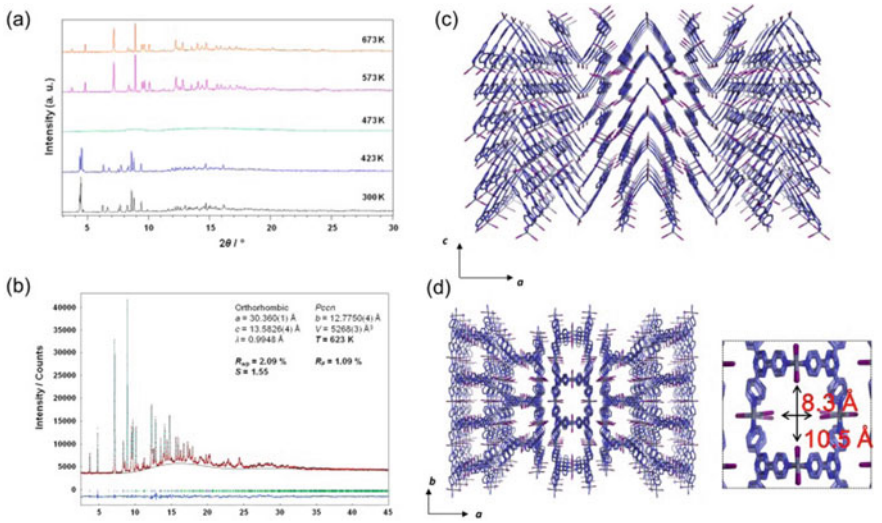

Fig. 12.3 **a** PXRD patterns of the kinetically assembled, interpenetrating network $[(ZnI_2)_3(TPT)_2]$ at different temperatures. It shows a crystalline-to-amorphous phase transition at 473 K and an amorphous-to-crystalline phase transition at 573 K. (Middle) **b** Rietveld refinement of the saddle network. **c**, **d** Crystal structures of the saddle network, $[(ZnI_2)_3(TPT)_2]$ with pore dimensions. Reproduced with permission of the American Chemical Society

phase transition upon heating [44–46]. The metastable state was converted to more stable states with increasing temperature. The microcrystals of the kinetic interpenetrating network were heated from 300 to 673 K and monitored by in situ synchrotron PXRD and TG-DSC. The diffraction showed crystalline-to-amorphous and amorphous-to-crystalline phase transitions at 473 and 673 K, respectively (Fig. 12.3a). Recently, we found that there are in fact two distinct amorphous phases occurring between the initial and final crystalline states. Therefore, the entire transformation sequence was denoted as CAAC phase transition. These types of transitions are rare in porous coordination networks. The closest related example was observed in some zeolitic imidazole frameworks (ZIFs), which underwent a two-step CAC transition [47–49].

The new crystalline state obtained by heating of the amorphous phase was different from the initial network structure and was thermally stable up to 673 K. The crystal structure was unambiguously determined by ab initio PXRD analysis, which showed that it has retained the molecular formula of $[(ZnI_2)_3(TPT)_2]$ (Fig. 12.3). In this new network, two TPT ligands are connected through two ZnI_2 units forming a "saddle" structure, which extended along the *b*-axis as 1D chains, thus, it was denoted as a "saddle network" (Fig. 12.3a–d). Adjacent chains are held together by intermolecular π–π interactions between stacked pyridyl and triazine rings along the *c*-axis giving rise to non-interpenetrating 1D channels with the dimensions of 6.2 × 8.5 Å. Due to its high thermal and structural stability, the saddle network could be used to encapsulate

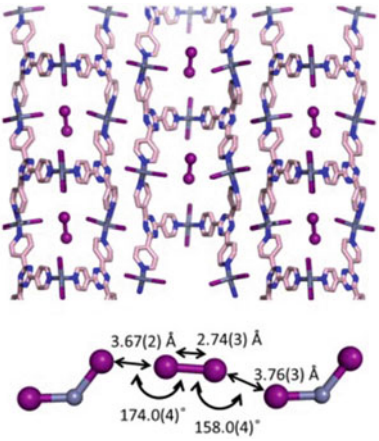

Fig. 12.4 (Top) Crystal structure of I_2-encapsulating saddle network, $I_2@[(ZnI_2)_3(TPT)_2]$. (Bottom) Interaction of the guest I_2 with the ZnI pore sites. Reproduced by permission of The Royal Society of Chemistry

guests by liquid–solid and gas–solid inclusion reactions. The isostructural network, $[(ZnBr_2)_2(ZnCl_2)(TPT)_2]$, was obtained by the solid–liquid interface reaction [50].

The structural transformation in the CAAC phase transition involves unlocking of the initial interpenetrating (10,3)-*b* network and its rearrangement into a 1D chain. First, guest removal and shrinking of the network occurs, followed by the opening of the 3D nets through cleavage of coordination bonds. After the chain rearrangement and the bond re-formation, the saddle network is obtained.

This type of thermal annealing can produce highly crystalline materials that are commonly used as ceramics and zeolites. This method was also applied to ZIF networks. When ZIF-4 ($[Zn(im)_2]$, im = imidazolate) was heated at 573 K, it changed to an amorphous phase, and further heating at 673 K produced another crystalline ZIF polymorph with different topology. The structure of the amorphous phase was a SiO_2 glass-like structure confirmed by pair distribution function analysis [47].

An important feature of the saddle structure is that the terminal iodide coordinating to Zn(II) faces into the pore (Fig. 12.3a–d). A guest molecule that enters the channel could interact with these iodide sites. For example, iodine can be physisorbed into the network, facilitated by halogen–halogen interactions (Fig. 12.4) [51]. The near-linear geometry between the network iodide and the guest I_2 molecules indicates a typical halogen–halogen interaction between positive (σ-hole) and negative sites (unpaired electrons) [52].

12.1.4 Interactive Pores in the Saddle Structure

Because the pores in the saddle network are decorated with terminal iodide groups creating interactive sites, they can be used for host-guest related applications, such as I_2 encapsulation. Due to this feature, the open structure was expected to function as a crystalline molecular flask, which could be used to monitor chemical reactions

directly by X-ray analysis [53–61]. Therefore, we decided to use the crystalline powder of this network for this role and selectively trap metastable and reactive species [62].

The small sulfur allotropes, S_n ($n < 6$), are unstable and cannot be isolated from the allotrope mixture either in the gas phase or in a solid Ar matrix [63–65]. These sulfur species are highly reactive and readily condense into heavier allotropes under ambient conditions. Therefore, their structures cannot be determined directly by X-ray diffraction. To overcome this issue, we trapped these unstable species inside a crystal matrix using the crystalline molecular flask method. We used interactive pore sites in the saddle porous coordination network, $[(ZnI_2)_3(TPT)_2]$, where the pore facing iodide groups could interact with the guest sulfur atoms and stabilize the reactive species.

Sulfur was encapsulated in the saddle network structure by vapor diffusion at 533 K under vacuum for 6 h. Under these conditions, the gaseous sulfur and the host network were fully equilibrated. After this treatment, the pale-yellow network powder turned bright yellow accompanied by change in the PXRD pattern. The changes in the peak positions and their relative intensities suggested that sulfur was successfully encapsulated into the network pores (Fig. 12.5).

Herein, we describe the structure determination procedure for the sulfur species, which were identified by ab initio PXRD analysis. After sulfur encapsulation, the crystal system of the network changed from *P*ccn with $a = 30.690$ Å, $b = 12.775$ Å, $c = 13.5826$ Å to *P*n with $a = 30.690$ Å, $b = 6.595$ Å, $c = 12.824$ Å, $\beta = 91.558°$. The structure of the sulfur-encapsulating network was solved by ab initio PXRD analysis using synchrotron data. First, the structure was solved using the model of the original network and several combinations of individual sulfur atoms to obtain the initial structural information about the possible sulfur allotropes. All solutions showed the presence of a S_3 moiety inside the pore of the coordination network. Using a S_3 model obtained from rotational spectroscopy experiments, [66] the ab initio PXRD analysis was repeated. The structure was further refined by the Rietveld method using the S_3-encapsulating model with soft restraints for the geometrical parameters.

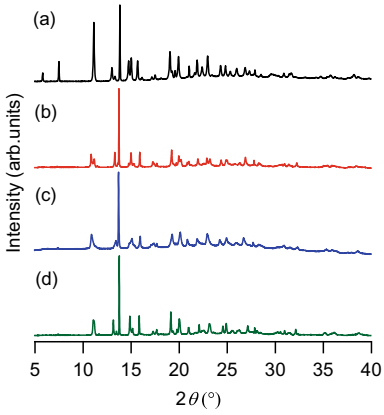

Fig. 12.5 RXPD pattern of the saddle network, **a** before sulfur encapsulation, **b** S_3-encapsulating network, **c** S_6-encapsulating network, and **d** sulfur polymer-encapsulating network. Reproduced with permission of the American Chemical Society

The good agreement between the experimental and calculated diffraction patterns indicated that the structure was correct. The X-ray diffraction analysis and elemental analysis revealed that discreet S_3 species were selectively trapped in the network pores (Fig. 12.6).

This example represents the first crystal structure determination of a reactive sulfur allotrope smaller than S_6. The open-triangle C_{2v} structure of the observed S_3 agreed well with structures obtained by rotational spectroscopy [66]. The sulfur molecule in the pore was disordered over two positions. Notably, the short interatomic distances between sulfur and iodide in the major component of S_3 were 3.1 and 3.3 Å, which were considerably shorter than the sum of their van der Waals radii (3.8 Å), indicating a strong interaction between them (Fig. 12.7). It was postulated that this interaction enabled the encapsulation and stabilization of, otherwise, reactive S_3 molecule.

The presence of S_3 in the pores was additionally confirmed spectroscopically from the characteristic shoulder peak in the vibrational spectrum at about 680 cm^{-1}, which corresponds to the S_3 asymmetric stretching. The encapsulated sulfur species exists in a neutral state, which was determined by the assignment of IR peaks and lack of a signal in the electron spin resonance spectrum.

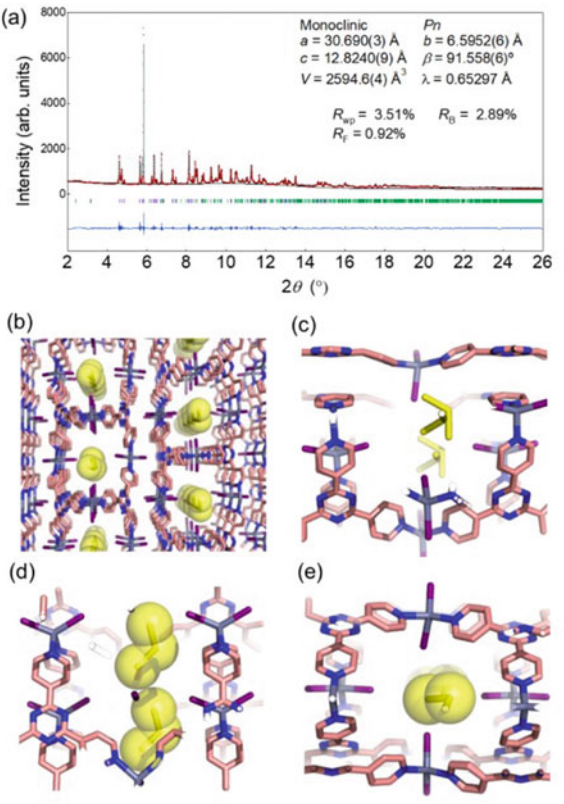

Fig. 12.6 Ab initio PXPD analysis of the S_3-encapsulating network. **a** Rietveld refinement and **b**–**e** crystal structure of the S_3-encapsulating network. Reproduced with permission of the American Chemical Society

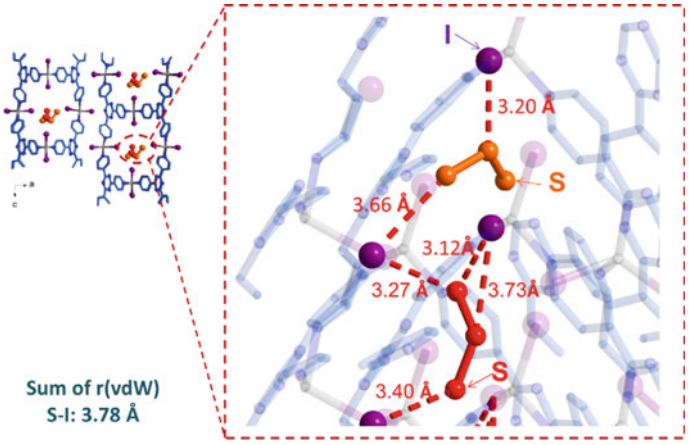

Fig. 12.7 Interaction of S_3 with interactive pore sites. The distances between S and I show important interactions. Reproduced by permission of The Royal Society of Chemistry

The S_3 encapsulated in the pores was remarkably stable because of the interaction with the pore facing iodide sites (Fig. 12.7). The PXRD pattern of the S_3-encapsulating network powder did not change significantly over 3 months of the exposure to ambient atmosphere. Thermogravimetric analysis of the host-guest material showed a weight decrease at temperatures above 500 K, which indicated that sulfur evaporation from the pores occurred at higher temperatures. Furthermore, the S_3 molecule inside the network was found to be inert to photo-irradiation oxidation conditions. These results further highlight the remarkable stabilization of the S_3, an analogue of ozone, inside the interactive pores of the saddle network.

Nevertheless, the encapsulated S_3 exhibited a unique reactivity. When the crystalline network powder was heated with NH_4Cl at 473 K for 6 h under vacuum, the PXRD pattern changed, indicating a structural transformation. The crystal structure determined by ab initio PXRD analysis showed that there were now 0.5 S_6 molecules in each pore (Figs. 12.5 and 12.8). The product of this transformation was six-membered rings with a chair conformation, which is characteristic of discrete S_6 molecules [63]. This result suggests that the S_3 in the pores dimerized to produce S_6 as follows:

$$S_3 + S_3 \rightarrow S_6$$

In the crystal structure, the encapsulated S_6 also interacts with network iodide as evidenced in the interatomic distances between sulfur and iodide (3.1 and 3.4 Å), which are shorter than the sum of their van der Waals radii (3.8 Å). The close proximity between S_6 and iodide indicates the presence of strong host–guest interaction, similar to the S_3. S_6 itself cannot enter the pore from outside because the diameter of the opening aperture is too small. Therefore, the only way to encapsulate S_6 is a ship-in-a-bottle approach [67] starting from smaller sulfur allotropes, like S_3.

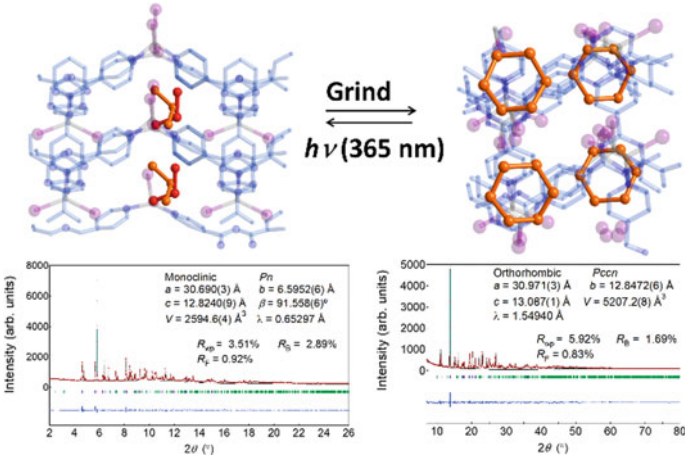

Fig. 12.8 Ab initio XRPD snapshots of the transformation of S_3 to S_6. Reproduced by permission of The Royal Society of Chemistry

However, the S_3 dimerization could not be achieved by simple heating, and NH_4Cl was required to catalyze the transformation. NH_4Cl is an impurity remaining from the ligand synthesis and acts as proton donor (Scheme 12.1) [68]. It is proposed that the hydrogen-bonding brings the sulfur trimers closer together allowing for cyclization to take place. Furthermore, the same structural transformation could be induced by mechanical action when grinding the S_3-encapsulating network powder, indicating the flexibility of the saddle structure.

Interestingly, this transformation could be reversed by excitation at 365 nm, fully recovering the starting S_3 molecules. This result indicates that inside the pore, S_3 is more stable toward light irradiation than S_6 (Fig. 12.8).

Overall, the interactivity of the pores was the key for efficient trapping of small sulfur allotrope and its conversion, helping to uncover the chemistry of these rare sulfur species.

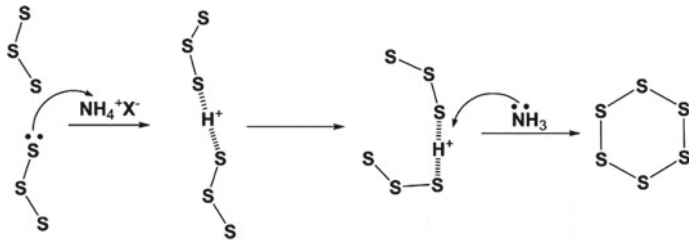

Scheme 12.1 Transformation of $2S_3$ to S_6 catalyzed by NH_4Cl

12.1.5 Encapsulation of Reactive Molecules, P_4 and Br_2

In addition, we used the saddle network to capture and stabilize other reactive elemental species, namely P_4, also known as white phosphorous, and Br_2 [69, 70]. Phosphorus tetramer was encapsulated into the pores using phosphorus vapor created by heating red phosphorus. The P_4 trapping was confirmed by X-ray diffraction, as shown in Fig. 12.9. This species was stabilized by weak interaction with the pore walls and was stable under air at 300 K. This means that this network can be used as a versatile P_4 container. The removal and re-trapping processes could be repeated, which is important for the molecular flask reusability. The presence of interactive sites inside the coordination network was demonstrated to be, once again, crucial for efficient trapping and release of reactive species. As a result, chemically and thermally robust porous networks can be used as facile and reusable reagent containers.

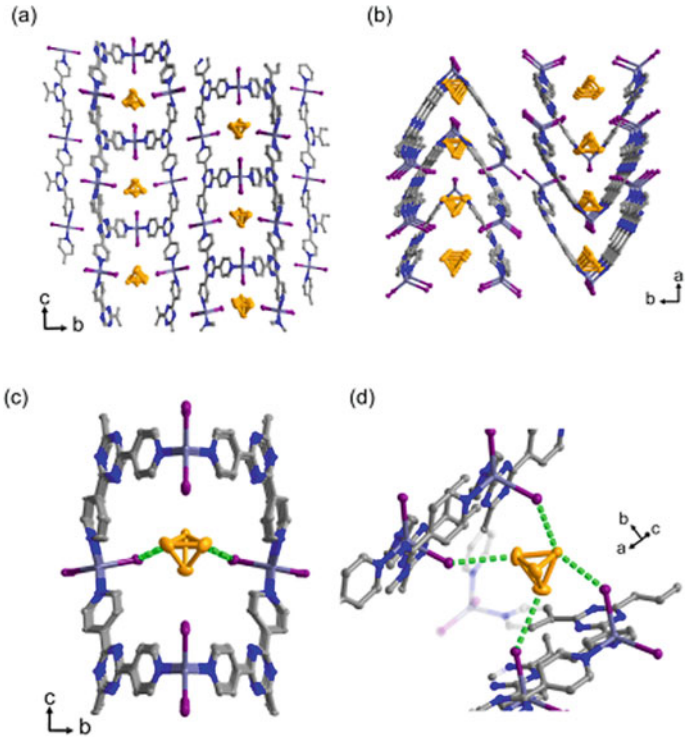

Fig. 12.9 Crystal structures (ORTEP plots, 50% probability) of single-crystal P_4@network **1** at 100 K: **a** view along *b*-axis, **b** view along *c*-axis, **c** pore description green dotted lines show interactions, **d** interaction between P_4 and iodides. Color codes: C, gray; N, blue; P, orange; Zn, pale-blue; and I, purple. Reproduced by permission of The Royal Society of Chemistry

12.1.6 Br_2 Encapuslation

To further investigate the trapping ability of the saddle network, we performed bromine encapsulation to determine whether Br_2 can be safely stored inside [70]. During this investigation, it was found that instead of just simply encapsulating Br_2 through physisorption, the oxidation of coordinated iodide had occurred, producing I_2. Furthermore, this reaction caused the displacement of iodide by bromide in the coordination sphere of Zn(II), giving rise to the ZnBr-based network containing I_2 as a guest:

$$\left[(ZnI_2)_3(TPT)_2\right] + 3Br_2 \rightarrow \left[(ZnBr_2)_3(TPT)_2(I_2)\right] + 2I_2$$

The new structure was confirmed by ab initio PXRD analysis (Fig. 12.10). The trapped I_2 showed strong interactions with the pore of the ZnBr network.

Additional evidence for the presence of I_2 inside the network was provided by Raman spectroscopy [71–73]. The Raman spectrum showed sharp peaks at 174 and 194 cm^{-1}, corresponding to I_2 encapsulated in the pore and I_2 attached to the

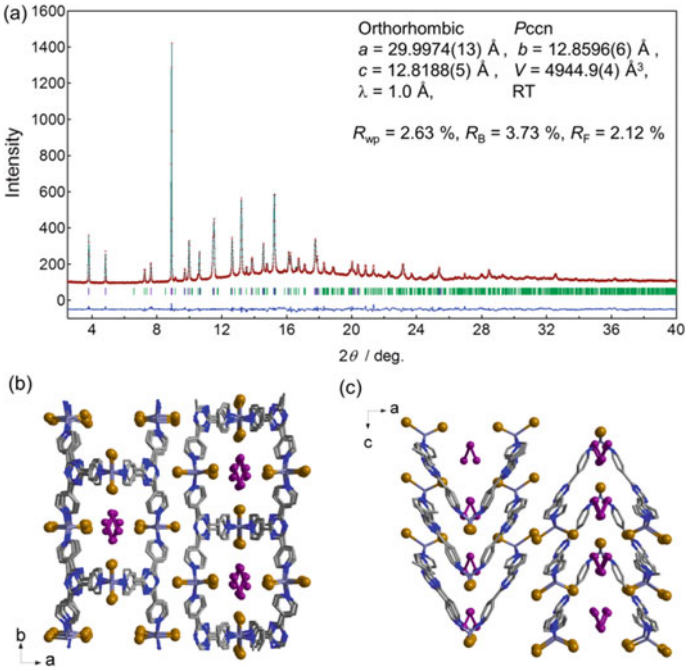

Fig. 12.10 Experimental (red), calculated (black), and difference (blue) PXRD profiles from the final Rietveld refinement of the I_2@$[(ZnBr_2)_3(TPT)_2]$. Crystal structure: **b** view along the *c*-axis. I_2 (occupancy 0.5) occupies two symmetrically related positions. **c** View along the *b*-axis. Color codes: C, gray; N, blue; Zn, pale-blue; I, purple; and Br, brown. Reproduced by permission of The Royal Society of Chemistry

surfaces of crystals, respectively. The presence of surface-confined iodine could not be avoided because the reaction produces two additional equivalents of I_2 which escapes the pores. The elemental analysis results determined the chemical formula of the network product to be $[(ZnBr_2)_3(TPT)_2(I_2)](I_{2\text{-surface}})_{0.67}$. The iodine loading was also quantified by TGA, which showed a two-step weight loss. The first step corresponds to desorption of I_2 from the particle surface, whereas the second one corresponds to the loss of I_2 from the pores. The overall weight decrease below 575 K was approximately 25.3%, which agrees with the total iodine content (24.6%) calculated from the molecular formula, $[(ZnBr_2)_3(TPT)_2(I_2)](I_{2\text{-surface}})_{0.67}$. The I_2 in the pore interacts with the Br^- sites of the network. The I···Br distance is 3.61 Å, which is shorter than the sum of the individual van der Waals radii of I and Br (3.75 Å) [74]. Also, the I–I–Br angle is 153° (non-linear), indicating mainly a π-type interaction combined with some contribution of σ-type interactions. The appearance of absorption band at 280 nm can be attributed to a strong charge-transfer interaction between Br^- and I_2. This band was not clearly observed in the $[(ZnI_2)_3(TPT)_2]$ network containing encapsulated I_2, indicating that only σ-type interactions occur between I^- sites of the network and the guest I_2. The brominated network shows significantly stronger affinity for I_2 because of the additional contribution of π-interactions which are absent in the iodine analogue.

This post-synthetic modification of the pore is due to the strong oxidative ability of Br_2. The oxidation potential of Br_2/Br^- redox couple is 1.087 V versus SHE, which is higher than that for the I_2/I^- couple, 0.54 V versus SHE. Therefore, the encapsulated of Br_2 readily oxidizes the constituent I^- to give I_2. This type of post-synthetic reaction is the first example of redox induced ligand transformation, which results in a network component replacement. The resulting pore modification enables the dramatic changes in the properties of interactive sites by switching from I^- to Br^-.

Furthermore, thermal treatment of the I_2 encapsulated ZnBr network led to the guest removal affording an activated structure. When the I_2 loaded $[(ZnBr_2)_3(TPT)_2]$ network was heated at 573 K, the powder turned white, which is a sign of the release of I_2 molecules from the pores. The ab initio PXRD structural analysis of the remaining white powder revealed it to be isostructural with the starting $[(ZnI_2)_3(TPT)_2]$ network (Fig. 12.11). The pore window of the bromine structure is 2.6 × 4.6 Å, which is larger compared to the iodide analogue because of the smaller ionic radius of Br^- relative to I^-. The halide replacement retained the overall saddle-type network structure and preserved the topology. The same structure could not be obtained starting directly from $ZnBr_2$ and TPT, either using a solution-phase synthesis or by crystallization from vapor. In both cases, the interpenetrating network was the predominant product. As a result, the only available synthetic route toward the $[(ZnBr_2)_3(TPT)_2]$ material is through oxidative encapsulation and ligand replacement with Br_2. The resultant bromide network was found to be stable up to 673 K under N_2, as confirmed by TGA measurements.

Due to the presence of Br^- ions as interactive pore sites, the trapping of Br_2 was attempted. For these experiments, the Br_2 vapor diffusion was also performed under the same conditions as those used for the Br_2 encapsulation into $[(ZnI_2)_3(TPT)_2]$.

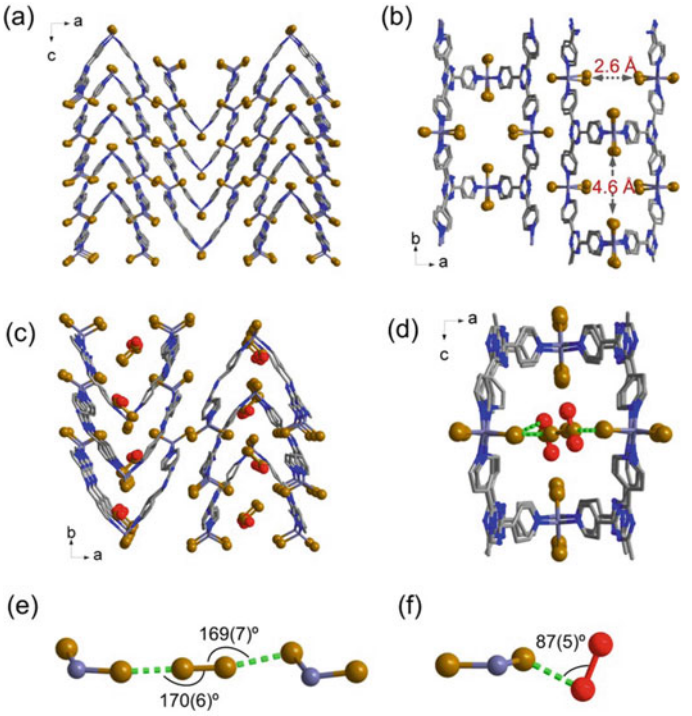

Fig. 12.11 Crystal structure of $[(ZnBr_2)_3(TPT)_2]$: **a** view along the *b*-axis, **b** view along the *c*-axis. Crystal structure of $Br_2@[(ZnBr_2)_3(TPT)_2]$: **c** view along the *c*-axis, **d** view along the *b*-axis. Green dotted lines show interactions. **e** Linear interactions between Br_2 and Br^- ions. **f** Perpendicular interactions between Br_2 and Br^- ions. Color codes: C, gray; N, blue; Zn, pale-blue; and Br, brown and red to distinguish disordered molecules. Reproduced by permission of The Royal Society of Chemistry

After the vapor exposure the bromide network powder changed color from white to yellow accompanied by the change in the PXRD pattern. The ab initio PXRD structural analysis of the resultant yellow powder revealed that the material has retained its basic ZnBr network structure while also incorporating the disordered Br_2 guests. These were physically adsorbed into the pore, strongly interacting with the network bromide groups. The observed Br$\cdots$Br distances were 3.44, 3.55, and 3.22 Å, shorter than the sum of the van der Waals radii of Br (3.70 Å). One of the disordered Br_2 molecules exhibits an almost linear geometry (Fig. 12.11e), which is an indication of σ-type halogen–halogen interaction. In contrast, the other disordered Br_2 assumes an almost perpendicular geometry (Fig. 12.11f), a telltale sign of a π-type interaction featuring an elongated Br_2 bond (2.38(14) Å) [75]. Therefore, both σ-hole and π-orbitals-based interactions can occur between the guest Br_2 and the host Br^-. These results highlight the diversity of halogen bonding types that are possible inside the interactive pores, which presents an opportunity to generate and study unusual polynuclear halide species that cannot exist outside.

12.1.7 Kinetic Assembly Using a Labile CuI Unit

The success of S_3 encapsulation prompted us to design materials that contain intrinsic interactivity within their pores using the principles of kinetic assembly. To produce coordination networks under kinetic control, we employed labile metal connectors. If a metal can readily exchange ligands under the reaction conditions, usually in solution, it may generate several species during network formation because of the presence of several intermediate metal complexes. In particular, labile multinuclear metal clusters could give rise to multiple species existing simultaneously in solution. However, in most metal ions the intermediate state geometries are predictable, which limits the number of easily accessible structures for the network metal connectors.

Therefore, to demonstrate the kinetic control for network formation, we decided to utilize labile metal connectors instead of commonly used metal ions [41, 76]. These were combined using a rigid, highly symmetric ligand to produce structurally robust networks. For this study, $[Cu_4I_4(PPh_3)_4]$ was selected as a suitable metal precursor, because its central Cu_4I_4 cubane core is kinetically labile in solution and can be readily converted into other copper iodide clusters [77, 78]. For the ligand, tetra-4-(4-pyridyl)phenylmethane (tppm) was used, which possesses all the required characteristics, namely structural rigidity, thermal stability, and tetrahedral symmetry. Upon heating a suspension of $[Cu_4I_4(PPh_3)_4]$ and tppm in DMSO in air at 453 K for 30 min, a homogenous colorless solution was obtained. Depending on the cooling rate, two kinds of network crystals could be obtained. Rapid cooling (ca. 20 K min^{-1}, kinetic assembly) exclusively produced yellow needles with the formula $[(CuI)_2(tppm)]$ in 99% yield. In contrast, slow cooling (ca. 3 K min^{-1}, thermodynamic assembly) resulted in the formation orange prisms with the formula $[(Cu_2I_2)(tppm)]$ in 95% yield. Although these two networks had the exact same chemical composition, their connectivity and topology were markedly different. Therefore, these materials could be considered as structural isomers (Fig. 12.12).

The single-crystal structure analysis of the kinetic isomer revealed that CuI helical chains bridged by tppm ligands formed a non-interpenetrating porous network along the *c*-axis, where each Cu(I) ion is coordinated by two nitrogen atoms of tppm ligand and two bridging iodide groups. The helical chain network has 1D channels with pore windows of 5.8 × 5.5 Å and a 35% void space (without solvent) in the unit cell volume. The most important feature of this structure is that the bridging iodide in the connecting cluster faces into the 1D channel, and therefore can act as interactive pore site (Fig. 12.12a, c, e).

The crystal structure analysis of the thermodynamic isomer on the other hand, revealed that it has a quadruply interpenetrating network consisting of Cu_2I_2 dimer units and tppm ligands. The structure is a 4,4-connected grid with the PtS topology if the Cu_2I_2 dimer units are considered as square-planar sites and the central carbon atom of tppm as a tetrahedral node. In addition, this network contains 1D channels with pore windows of 4.0 × 3.9 Å and a 22% void space in the unit cell volume. The iodide groups in the Cu_2I_2 dimer are obscured by tppm ligands from the interpenetrating nets, which is different from the kinetic structure. As a result, the channels

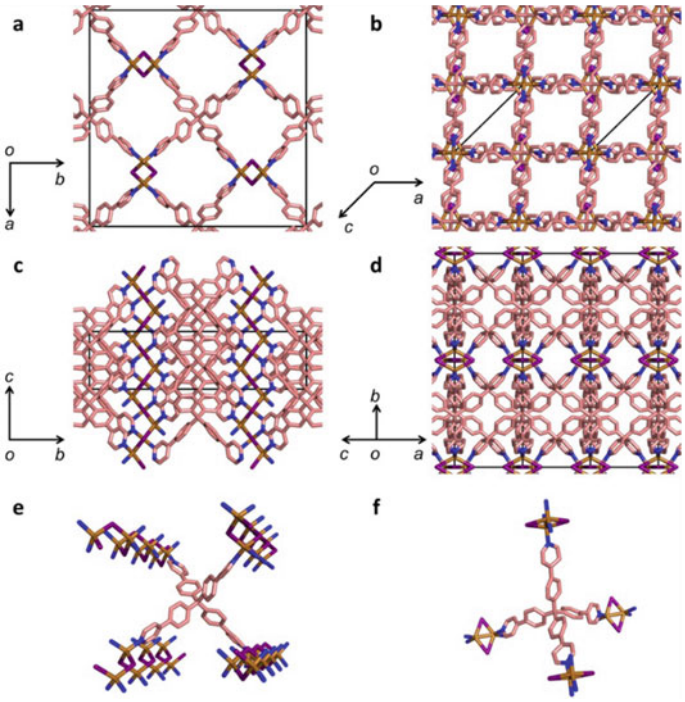

Fig. 12.12 Crystal structure of **a**, **c**, **e** kinetically assembled network, $[(CuI)_2(tppm)]$ and **b**, **d**, **f** thermodynamically assembled network isomer, $[(Cu_2I_2)(tppm)]$. Reproduced with permission of John Wiley and Sons

in the thermodynamic network are not decorated by the interactive iodide sites, and thus are relatively featureless (Fig. 12.12b, d, f).

The helical isomer can be converted to the dimer isomer by heating the powder in DMSO at 373 K for 1 day. This result confirms the kinetic nature of the helical network. On the other hand, the dimer network was found to be thermodynamically stable in a DMSO solution up to the decomposition temperature of DMSO.

The crystals of kinetic network exhibit higher stability in the solid state compared to solution. TGA showed that the decomposition temperatures of the two isomers were above 673 K under nitrogen atmosphere. More importantly, both networks crystals retained their crystallinity and porosity even after desolvation. It can be concluded that in solid state there is a very high energy barrier for the conversion of helical isomer into dimer structure. Due to this remarkable stability, the kinetic product could be suitable for practical solid-state applications.

To elucidate the properties of interactive pore sites, I_2 sorption experiments were performed on both solvated and desolvated networks. The sample crystallinity was retained after the I_2 exposure. Single-crystal structure analysis showed that the pores of the kinetic network encapsulated I_2 via chemisorption mechanism converting I^- groups in the connector units into linear I_3^- (Fig. 12.13a, b). In contrast, the ther-

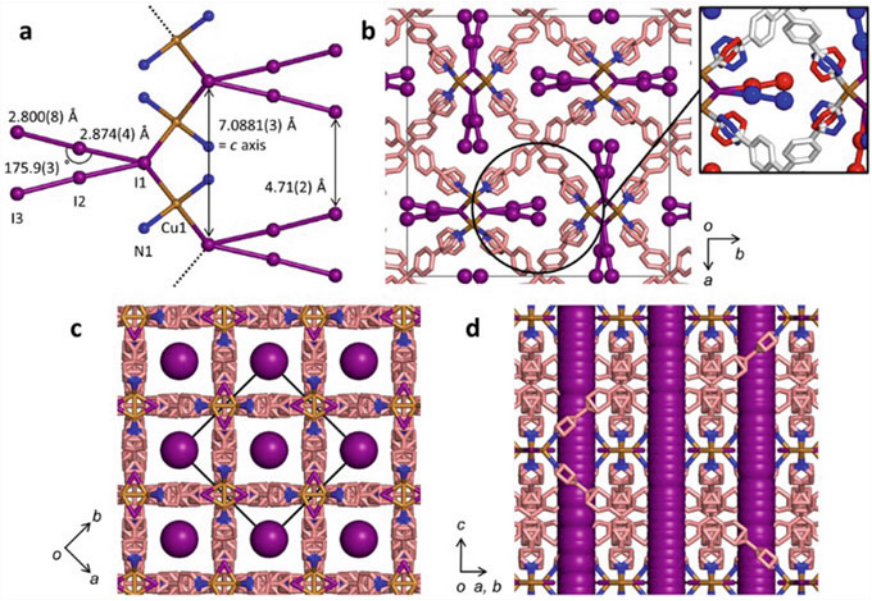

Fig. 12.13 Crystal structure of **a**, **b** chemisorption of I_2 (I_2@[$(CuI)_2$(tppm)]) and **c**, **d** physisorption of I_2 (I_2@[(Cu_2I_2)(tppm)]). Reproduced with permission of John Wiley and Sons

modynamic network only displayed physisorption of I_2 (Fig. 12.13c, d). The crystal structure analysis revealed that the I_2 molecules are arranged linearly along the 1D channels and are highly disordered, which is similar with I_2 physisorption in an organic zeolite and a phosphazene crystal [79, 80]. These results clearly demonstrate the importance of interactive pores in facilitating the chemical bond formation between bridging iodides and guest I_2.

Remarkably, even though I_2 formed chemical bonds with the pores of helical network, its desorption temperature was unexpectedly lower than for the physisorbed I_2 inside the dimer network. This behavior was attributed to the steric repulsion between adsorbed I_2 molecules and the framework backbone. In particular, the pyridyl ring rotation is expected to become more rapid with increasing temperature, which would cause the collisions with the I_3^- units leading to their displacement.

I_2 sorption was also investigated in solution by UV–Vis spectroscopy. The kinetics of I_2 sorption in cyclohexane solution revealed two distinct stages. Initially, a first-order sorption process is observed, suggesting physisorption, followed by a second-order sorption process, indicative of chemisorption.

The mechanism of kinetic network formation was investigated by nuclear magnetic resonance (NMR) spectroscopy. The NMR study revealed that oxygen is essential for the reaction. In anaerobic conditions, no network formation was detected. The NMR results helped to elucidate the mechanism. First, the PPh_3 group in the starting material, $[Cu_4I_4(PPh_3)_4]$, is removed by oxidation to produce

a vacant copper site and O = PPh_3. Second, DMSO rapidly occupies the coordinatively unsaturated site to generate a solvated CuI monomer at 453 K. Then, a tppm ligand coordinates to the resultant CuI monomer to generate the intermediate species, $[(CuI(DMSO)_2)_4(tppm)]$. The kinetic network can be crystallized from this intermediate complex by rapid cooling of the reaction mixture. The outlined kinetic assembly process is a powerful method for creating interactive pore sites in coordination networks.

12.1.8 S_2 Trapping in Thermodynamically Assembled Network

Because thermodynamic network has small pores, it can be particularly suitable for small sulfur allotrope encapsulation, similar to the studies described in Sect. 12.1.4. The small pore size cannot accommodate sulfur clusters larger than S_3, and it was expected to predominantly encapsulate disulfur, S_2. This favorable characteristic prompted us to conduct an in-depth study into sulfur encapsulation in the dimer network [81].

Sulfur was encapsulated from the gas phase by the kinetic trapping method, in which only sulfur vapor was present in the glassware while the network was kept at room temperature to create a temperature gradient (as described in Sect. 12.1.9).

X-ray structure analysis of the sulfur-containing network revealed that S_2 molecules were physisorbed at two different sites inside the channel: (i) Highly disordered along the length of the channel and (ii) within small cavities adjacent to the Cu_2I_2 units (Fig. 12.14).

Only the physisorption of S_2 was observed in the pore because of the steric hindrance around the iodide sites. The small size and linear shape of the 1D channels selectively trapped S_2 molecules and prevented further growth of larger sulfur allotropes. The presence of sulfur dimers in the network was confirmed by Raman spectroscopy at room temperature. A new band appeared at 728 cm^{-1} corresponding to the S_2 symmetric stretching mode. The encapsulated sulfur species remained stable inside the network up to 500 K because of the confinement effect of the pore.

The fact that the S_2 was detected in the pores implies that gas-phase sulfur incorporation in other porous networks proceeds predominantly via the sulfur dimers.

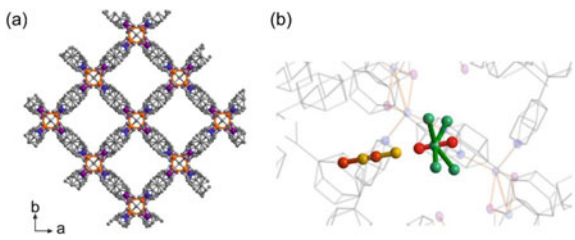

Fig. 12.14 Crystal structure of **a** desolvated CuI network, $[(Cu_2I_2)(tppm)]$ and **b** S_2-encapsulating $[(Cu_2I_2)(tppm)]$. Reproduced with permission of the International Union of Crystallography

This is consistent with the fact that the largest fraction of the gaseous sulfur is in its dimer state [65]. Therefore, S_3 encapsulation in the saddle $[(ZnI_2)_3(TPT)_2]$ network likely occurred via a ship-in-a-bottle cluster assembly. First, S_2 (disulfur) molecules enter the pores of the network and then are converted to S_3 (trisulfur) due to its higher stability. Since the encapsulation is conducted under the equilibrium conditions, it is difficult to determine the exact mechanism of disulfur molecule conversion. To observe these processes, the guest molecules should be kinetically trapped before the equilibrium state is reached. To achieve this, iodide sites could act as suitable interactive sites to capture small sulfur species and prevent their aggregation. To explore this possibility, we employed of kinetically assembled helical CuI network with interactive pores, as discussed in Sect. 12.1.7.

12.1.9 X-Ray Snapshots of the S_2 Conversion Inside an Interactive Pore

As mentioned in Sect. 12.1.4, pores lined up with interactive iodide sites could serve as efficient traps to stabilize and visualize small sulfur species. Furthermore, in Sect. 12.1.4, we also described sulfur encapsulation into the saddle ZnI network performed under equilibrium conditions. Elemental sulfur and the network powder were kept at 533 K under vacuum for 6 h to encapsulate sulfur gas. Because of the equilibrium conditions, it was difficult to determine the conversion mechanism before the sulfur species reached their equilibrium state inside the network pores. To overcome this limitation, kinetic trapping of small metastable sulfur allotropes was used to observe their conversion in the pore.

The CuI helical network was used for the trapping experiments due to the presence of interactive iodide sites where the sulfur transformation could occur. Unlike earlier encapsulation experiments, the sulfur trapping into the helical structure was carried out under kinetic conditions. Elemental sulfur and the desolvated network powder were placed at well-separated locations in a zig-zag glass tube, followed by sealing it under vacuum (~10^{-6} Torr). The sulfur side of the tube was heated to generate the sulfur vapor, while the network side was kept at the room temperature creating a sharp temperature gradient. This arrangement enabled the gaseous sulfur molecules to be trapped kinetically by the porous material. After the reaction was complete, single-crystal X-ray diffraction was performed on the resultant sample sequentially at 250, 300, 350, and again 250 K. The analysis of these diffraction patterns revealed the structure of transient small sulfur allotropes. The initial structure at 250 K showed the presence of two types of physisorbed guests in the network channels, S_2 and bent-S_3 species. Upon increasing the temperature to 300 K, the crystal structure analysis revealed the formation of cyclo-S_3 chemisorbed to the bridging iodide sites in addition to bent-S_3 and cyclo-S_3, both physisorbed in the channels. A theoretical investigation showed that the stronger interacting cyclo-S_3 species should be in its dicationic state, cyclo-S_3^{2+}. Further heating to 350 K resulted in the opening of the

cyclic trimers to give two kinds of bent-S_3 species, one still bound to the network iodide sites and the other physisorbed inside the pore.

From these X-ray diffraction experiments, a tentative reaction mechanism for the temperature-induced interconversion of sulfur species inside the helical CuI network is proposed. First, S_2 is kinetically trapped by rapid absorption into the pore and then partially transformed into bent-S_3 structure. Since the dimer was only detected at 250 K, it is a strong indicator that this allotrope is the starting point for the following conversion reactions. Second, on heating, S_2 converts to a number of trimeric species, namely chemisorbed cyclo-S_3^{2+} and physisorbed cyclo-S_3 and bent-S_3. After that, the cyclic forms underwent a ring opening to produce more stable bent-S_3 species (Fig. 12.15). Despite the kinetic nature of the experiments, the X-ray analysis results were generally reproducible.

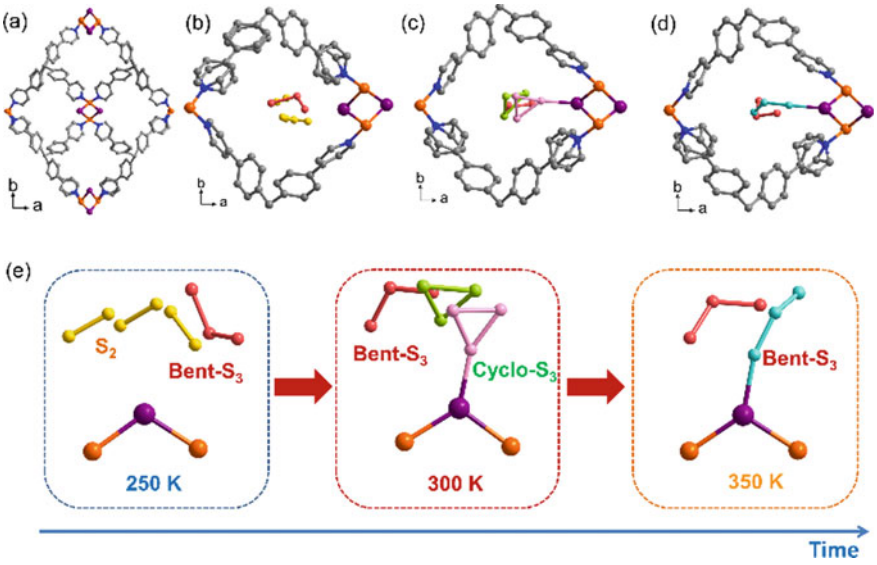

Fig. 12.15 Pore description in crystal structure of **a** the CuI helical network, $[(CuI)_2(tppm)]$, **b** helical network after sulfur encapsulation at 250 K, **c** 300 K and **d** 350 K. **e** The crystal structure of sulfur-encapsulating helical network showing parts of {CuI} unit and sulfur species. At 250 K, physisorbed S_2 and bent-S_3 were observed (left), at 300 K, chemisorbed cyclo-S_3^{2+}, physisorbed cyclo-S_3 and bent-S_3 were observed (middle), and at 350 K, bent-S_3 was observed. Blue arrow indicates the time course of the measurements showing molecular transformation mechanism from S_2 to bent-S_3 species. Atoms coloring: Cu, orange; I, purple, S, yellow, red, green, pink and cyan to distinguish disordered molecules. Reproduced with permission of the International Union of Crystallography

12.1.10 Identifying Cyclo-S_3 Species in the Pore

Theoretical calculations predicted that cyclo-S_3 is less stable than bent-S_3, yet energetically accessible. However, its experimental observation had never been reported before. Hoffman used DFT calculations to show that the neutral form of cyclo-S_3 is 5.6 to 9.3 kJ/mol less stable than bent-S_3, depending on the calculation method [82]. Therefore, the cyclic form was predicted to be a metastable state. Indeed, the interactive pores were able to temporarily trap cyclo-S_3 as an intermediate species. This result represents the first structure of a cyclic S_3 allotrope determined using single-crystal X-ray diffraction. The cyclo-S_3 was stabilized through a chemical bond formation to create an I-(cyclo-S_3^{2+}) complex. Furthermore, the dication of the cyclic trimer is the isoelectric state to a cyclo-SiS_2 molecule isolated by matrix isolation, supporting the possibility of cyclo-S_3^{2+} existence [83]. The structural analysis of the metastable sulfur allotrope trapped by the pore of the coordination network opens up new avenues for producing and characterizing unusual sulfur species.

12.1.11 Theoretical Investigation of Sulfur Allotropes in the Pores

The ability of interactive pore sites to trap and stabilize small sulfur allotropes was investigated using theoretical calculations. Since both physisorbed and chemisorbed S_2 species appeared in the same structure, the energetics of the chemisorption process and electronic spin changes were evaluated. To obtain this information, the energy of the $I^- \cdots S$–S complex was calculated.

In a triplet electronic state, the S_2 molecule is only physisorbed onto the iodide. The interaction energy of this intermolecular interaction was calculated to be −29.2 kJ/mol with the I–S bond order of 0.1294. As a result, this intermolecular interaction cannot be considered as a covalent bond and is more similar in strength to a halogen bond. The formation of this weakly interacting complex involves charge transfer from the iodide primarily to the furthest sulfur atom. The equilibrium distance for this interaction is 3.317 Å and the resultant species has a bent geometry with a $I \cdots S$–S angle of 127.5°.

On the other hand, in the singlet electronic state (Table 12.1 and Fig. 12.16), the S_2 molecule is chemisorbed onto the iodide. In the process, a covalent I–S bond is formed with a bond order of 0.9293 and the bond distance of 2.602 Å. The geometry of chemisorbed complex is also bent, with an I–S–S angle of 112.5°. In addition, there is a considerable charge transfer from the iodide to the sulfur atoms. The I–S–S Mulliken charges are −0.372, −0.144, and −0.484, respectively. The distant sulfur atom receives the highest negative charge. From these results, it can be concluded that a donor-acceptor bond forms between the iodide and the sulfur atom. However, the total energy gain in creating this intramolecular bond is only −19.4 kJ/mol, almost 10 kJ/mol less stabilizing than physisorption.

Table 12.1 Stability and key structural parameters for the optimized $I^{-}\cdots S_2$ complex in the triplet and singlet spin states

	$I^{-}\cdots S_2$	
Spin	Triplet	Singlet
Nature	Physisorption	Chemisorption
d(I–S) in Å	3.317	2.602
Wiberg I–S bond order	0.1943	0.9293

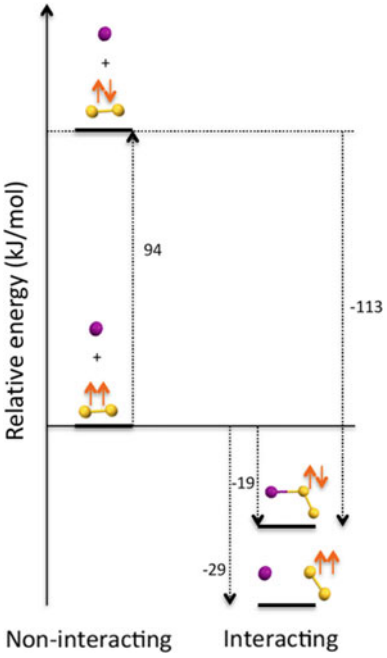

Fig. 12.16 Schematic of the stability of the interacting $I^{-}\cdots S_2$ with respect to the isolated species in the singlet and triplet spin states. Reproduced with permission of the International Union of Crystallography

Chemisorption is energetically less favorable than physisorption in this system because the triplet-to-singlet spin conversion is required for this process. The relative energies of the various (isolated, non-interacting, and interacting) systems are shown in Fig. 12.16.

In isolation, the triplet spin state of the S_2 molecule is considerably more stable than the singlet state by approximately 94 kJ/mol. Therefore, when the sulfur gas was produced for the encapsulation experiment, it likely mostly consisted of triplet dimers. In the presence of the iodide groups however, both the chemisorbed singlet and the physisorbed triplet states have similar energies. They differ by only 10 kJ/mol. With respect to the isolated S_2 triplet state, the singlet chemisorbed S_2 is only

19 kJ/mol more stable. In comparison, the singlet chemisorbed S_2 state is 113 kJ/mol more stable relative to its isolated form and is in the order of a covalent bond. These results unambiguously explain that the lower stability and generally weaker binding of the chemisorbed sulfur dimer compared to the physisorbed species is due to the energy of the spin transition. Therefore, the physisorption process is more favorable for S_2 encapsulation in the pores.

In addition, the reaction pathway from the physisorbed triplet S_2 to the chemisorbed singlet S_2 was examined. Figure 12.15 shows that the I–S bond formation process has an energy barrier of 15 kJ/mol. The transition state occurs at around $I^- \cdots S$ distance of 2.8 Å (Fig. 12.17).

Finally, the properties of the intermediate cyclo-S_3 species were calculated. The calculated structure of chemisorbed cylco-S_3^{2+} showed that the bond lengths in the sulfur-iodine complex were closely matching with those determined by the X-ray structure analysis without any geometrical constraints or restraints (Fig. 12.18).

Structural information is essential for understanding chemical reactions and material properties. However, the difficulty in determining the structures of intermediate

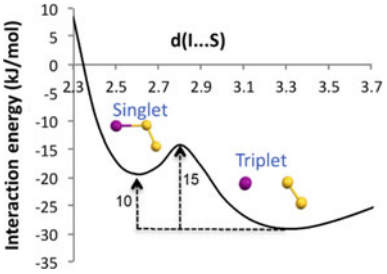

Fig. 12.17 Potential energy curve of the physisorption to chemisorption transition process of a molecule of S_2 onto an iodide atom in the gas phase. Reproduced with permission of the International Union of Crystallography

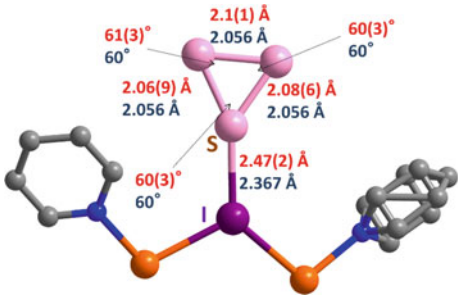

Fig. 12.18 Geometrical parameters from X-ray analysis and theoretical calculations for chemisorbed cyclo-S_3^{2+}. Red numbers refer to the values obtained from X-ray analysis, blue numbers refer to values obtained from the calculation of I-(cyclo-S_3^{2+}). Cu, orange; I, purple, and S, pink. Reproduced with permission of the International Union of Crystallography

and unstable species has hampered progress in their basic understanding. Herein, we demonstrated the advantages of using interactive pores to trap labile and unstable species and observe their reactivities by X-ray analysis. The representative example was the detection of metastable small sulfur allotropes and their interconversion for the first time inside the pores of the helical CuI network. Interactive pores used in these studies can be created by kinetic assembly of the coordination networks from their precursors. Application of this method to monitoring of catalytic transformations could lead to deeper understandings of their reaction mechanisms. These kinds of studies are crucial for the future design and development of novel functional materials.

12.1.12 Future Perspective

Self-assembly of coordination networks has been studied intensively by many researchers over the past quarter century. However, while the formation of kinetic side-products has been frequently noted, their detailed investigations have been scarce due to low stability and poor crystallinity. We demonstrated that kinetic assembly of porous coordination networks could be used to produce materials with interactive pore sites. The properties of these sites largely determine the possible applications of the kinetic materials.

One promising application for the interactive pore sites is trapping and visualization of unstable species. The range of potential unstable allotropes than can be targeted is broad and includes sulfur, phosphorus, and selenium among others. For example, in the case of phosphorus, only it is more widely known and a more stable form, P_4, was encapsulated in the interactive pores. However, there are still no examples of stabilization and visualization of elusive dimer, P_2, even though it is known to exist at high temperatures, and has the same electronic configuration as N_2. Therefore, this phosphorus allotrope could be a highly interesting candidate for the future encapsulation studies.

Another intriguing application is the control of transition states. If an interactive pore could behave like an enzyme pocket, it could be used to modulate transition states of various transformations. Achieving such degree of control could open up new reaction pathways that cannot be reached with the conventional methods. In addition, interactive sites could also function as active catalytic centers, if their interactions with a substrate lower the activation energy. Therefore, the design and construction of the desired interactive sites from suitable metal connectors and ligands could present and powerful approach for the development tailor-made catalysts. Some of the best catalytic systems in existence, natural enzymes, utilize interactive sites extensively in their functions. These systems enable unprecedented acceleration of otherwise difficult reactions, such as methane monooxygenase (MMO), which oxidizes methane to methanol. Our ultimate goal is to develop such bio-mimetic catalysts by utilizing interactive sites generated in kinetically assembled networks.

In this sense, the careful design of desired interactive sites is a key step toward building materials that mimic biological functions, particularly the ability to catalyze reactions under mild conditions. This task will be accomplished by the judicious development of multifunctional ligands, the selection of appropriate metal connectors, and tuning the reaction parameters. However, there are still many challenges that need to be addressed before the kinetically assembled coordination networks could come close to reaching such a formidable goal.

References

1. Dichtel, W.R., Miljanić, O.Š., Zhang, W., Spruell, J.M., Patel, K., Aprahamian, I., Heath, J.R., Stoddart, J.F.: Kinetic and thermodynamic approaches for the efficient formation of mechanical bonds. Acc. Chem. Res. **41**, 1750–1761 (2008)
2. Dickson, A., Brooks III, C.L.: Native states of fast-folding proteins are kinetic traps. J. Am. Chem. Soc. **135**, 4729–4734 (2013)
3. Hua, Q.X., Gozani, S.N., Chance, R.E., Hoffmann, J.A., Frank, B.H., Weiss, M.A.: Structure of a protein in a kinetic trap. Nat. Struct. Biol. **2**, 129–138 (1995)
4. Cheetham, A.K., Rao, C.N., Feller, R.F.: Structural diversity and chemical trends in hybrid inorganic–organic framework materials. Chem. Commun. **46**, 4780–4795 (2006)
5. Zhu, Y., Hua, Z., Zhou, J., Wang, L., Zhao, J., Gong, Y., Wu, W., Ruan, M., Shi, J.: Hierarchical mesoporous zeolites: direct self-assembly synthesis in a conventional surfactant solution by kinetic control over the zeolite seed formation. Chem. Eur. J. **17**, 14618–14627 (2011)
6. Wang, Y., Gao, X., Xiao, Y., Zhao, Q., Yang, J., Yan, Y., Huang, J.: Temperature dependent coordinating self-assembly. Soft Matter **11**, 2806–2811 (2015)
7. Zhong, Q.Z., Li, S., Chen, J., Xie, K., Pan, S., Richardson, J.J., Caruso, F.: Oxidation-mediated kinetic strategies for engineering metal-phenolic networks. Angew. Chem. Int. Ed. **58**, 12563–12568 (2019)
8. Michele, L.D., Varrato, F., Kotar, J., Nathan, S.H., Foffi, G., Eiser, E.: Multistep kinetic self-assembly of DNA-coated colloids. Nat. Commun. **4**, 2007 (2013)
9. Batten, S.R., Robson, R.: Interpenetrating nets: ordered, periodic entanglement. Angew. Chem. Int. Ed. **37**, 1460–1494 (1998)
10. Eddaoudi, M., Moler, D.B., Li, H., Chen, B., Reineke, T.M., O'Keefe, M., Yaghi, O.M.: Modular chemistry: secondary building units as a basis for the design of highly porous and robust metal–organic carboxylate frameworks. Acc. Chem. Res. **34**, 319–330 (2001)
11. Kitagawa, S., Kitaura, R., Noro, S.: Functional porous coordination polymers. Angew. Chem. Int. Ed. **43**, 2334–2375 (2004)
12. Kitagawa, S., Uemura, K.: Dynamic porous properties of coordination polymers inspired by hydrogen bonds. Chem. Soc. Rev. **34**, 109–119 (2005)
13. Bradshaw, D., Claridge, J.B., Cussen, E.J., Prior, T.J., Rosseinsky, M.J.: Design, chirality, and flexibility in nanoporous molecule-based materials. Acc. Chem. Res. **38**, 273–282 (2005)
14. Kawano, M., Fujita, M.: Direct observation of crystalline-state guest exchange in coordination networks. Coord. Chem. Rev. **251**, 2592–2605 (2007)
15. Férey, G.: Hybrid porous solids: past, present, future. Chem. Rev. **37**, 191–214 (2008)
16. Furukawa, H., Cordova, K.E., O'Keefe, M., Yaghi, O.M.: The chemistry and applications of metal-organic frameworks. Science **341**, 1230444 (2013)
17. Cook, T.R., Zheng, Y.R., Stang, P.J.: Metal-organic frameworks and self-assembled supramolecular coordination complexes: comparing and contrasting the design, synthesis, and functionality of metal-organic materials. Chem. Rev. **113**, 734–777 (2013)
18. Hoskins, B.F., Robson, R.: Infinite polymeric frameworks consisting of three dimensionally linked rod-like segments. J. Am. Chem. Soc. **111**, 5962–5964 (1989)

19. Hoskins, B.F., Robson, R.: Design and construction of a new class of scaffolding-like materials comprising infinite polymeric frameworks of 3D-linked molecular rods. A reappraisal of the zinc cyanide and cadmium cyanide structures and the synthesis and structure of the diamond-related frameworks $[N(CH_3)_4][Cu^{I}Zn^{II}(CN)_4]$ and Cu^{I}[4,4′,4″,4‴-tetracyanotetraphenylmethane]$BF_4 \cdot xC_6H_5NO_2$. J. Am. Chem. Soc. **112**, 1546–1554 (1990)
20. Fujita, M., Kwon, Y.J., Washizu, S., Ogura, K.: Preparation, clathration ability, and catalysis of a two-dimensional square network material composed of cadmium(II) and 4,4′-bipyridine. J. Am. Chem. Soc. **116**, 1151–1152 (1994)
21. Yaghi, O.M., Li, H.: Hydrothermal synthesis of a metal-organic framework containing large rectangular channels. J. Am. Chem. Soc. **117**, 10401–10402 (1995)
22. Kondo, M., Yoshitomi, T., Seki, K., Matsuzaka, H., Kitagawa, S.: Three-dimensional framework with channeling cavities for small molecules: $\{[M_2(4,4'\text{-bpy})_3(NO_3)_4] \cdot xH_2O\}_n$ (M = Co, Ni, Zn). Angew. Chem. Int. Ed. Engl. **36**, 1725–1727 (1997)
23. Riou, D., Serre, C., Férey, G.: Composite microporous compounds (MIL-n): II. Hydrothermal synthesis and ab initio resolution by X-ray powder diffraction of MIL-5: a vanadodiphosphonate with a three-dimensional neutral framework. J. Solid. State. Chem. **141**, 89–93 (1998)
24. Stock, N., Biswas, S.: Synthesis of metal-organic frameworks (MOFs): routes to various MOF topologies, morphologies, and composites. Chem. Rev. **112**, 933–969 (2012)
25. Zhang, J., Wojtas, L., Larsen, R.W., Eddaoudi, M., Zaworotko, M.J.: Temperature and concentration control over interpenetration in a metal–organic material. J. Am. Chem. Soc. **131**, 17040–17041 (2009)
26. Bara, D., Wilson, C., Mörtel, M., Khusniyarov, M.M., Ling, S., Slater, B., Sproules, S., Forgan, R.S.: Kinetic control of interpenetration in Fe-biphenyl-4,4′-dicarboxylate metal-organic frameworks by coordination and oxidation modulation. J. Am. Chem. Soc. **141**, 8346–8357 (2019)
27. Yang, S., Lin, X., Lewis, W., Suyetin, M., Bichoutskaia, E., Parker, J.E., Tang, C.C., Allan, D.R., Rizkallah, P.J., Hubberstey, P., Champness, N.R., Thomas, K.M., Blake, A.J., Schröder, M.: A partially interpenetrated metal–organic framework for selective hysteretic sorption of carbon dioxide. Nat. Mater. **11**, 710–716 (2012)
28. Yu, T., Wang, S., Li, X., Gao, X., Zhou, C., Cheng, J., Li, B., Li, J., Chang, J., Hou, H., Liu, Z.: Roles of temperature, solvent, M/L ratios and anion in preparing complexes containing a Himta ligand. CrystEngComm **18**, 1350–1362 (2016)
29. De, D., Neogi, S., Bharadwaj, P.K.: Stoichiometry controlled structural variation in three-dimensional Zn(II)–frameworks: single-crystal to single-crystal transmetalation and selective CO_2 adsorption. Cryst. Growth Des. **16**, 5238–5246 (2016)
30. Wee, L.H.H., Meledina, M., Turner, S., Van Tendeloo, G., Zhang, K., Rodriguez-Albelo, L.M., Masala, A., Bordiga, S., Jiang, J., Navarro, J.A.R., Kirschhock, C.E.A., Martens, J.A.: 1D–2D-3D transformation synthesis of hierarchical metal-organic framework adsorbent for multicomponent alkane separation. J. Am. Chem. Soc. **139**, 819–828 (2017)
31. Werner, J., Rams, M., Tomkowicz, Z., Runčevski, T., Dinnebier, R.E., Suckert, S., Näther, C.: Thermodynamically metastable thiocyanato coordination polymer that shows slow relaxations of the magnetization. Inorg. Chem. **54**, 2893–2901 (2015)
32. Forster, P.M., Burbank, A.R., Livage, C., Férey, G., Cheetham, A.K.: The role of temperature in the synthesis of hybrid inorganic–organic materials: the example of cobalt succinates. Chem. Commun. **4**, 368–369 (2004)
33. Näther, C., Bhosekar, G., Jess, I.: Preparation of stable and metastable coordination compounds: insight into the structural, thermodynamic, and kinetic aspects of the formation of coordination polymers. Inorg. Chem. **46**, 8079–8087 (2007)
34. Zhang, J.P., Huang, X.C., Chen, X.M.: Supramolecular isomerism in coordination polymers. Chem. Soc. Rev. **38**, 2385–2396 (2009)
35. Nagarkar, S.S., Chaudhari, A.K., Ghosh, S.K.: Role of temperature on framework dimensionality: supramolecular isomers of $Zn_3(RCOO)_8$ based metal organic frameworks. Cryst. Growth Des. **12**, 572–576 (2012)

36. Manna, B., Chaudhari, A.K., Joarder, B., Karmakar, A., Ghosh, S.K.: Dynamic structural behavior and anion-responsive tunable luminescence of a flexible cationic metal–organic framework. Angew. Chem. Int. Ed. **52**, 998–1002 (2013)
37. Bernini, M.C., de la Pena-O'Shea, V.A., Iglesias, M., Snejko, N., Gutiérrez-Puebla, E., Brusau, E.V., Narda, G.E., Illas, F., Monge, M.Á.: Thermodynamic and kinetic control on the formation of two novel metal-organic frameworks based on the Er(III) ion and the asymmetric dimethylsuccinate ligand. Inorg. Chem. **49**, 5063–5071 (2010)
38. Gándara, F., de la Pena-O'Shea, V.A., Illas, F., Snejko, N., Proserpio, D.M., Gutiérrez-Puebla, E., Monge, M.A.: Three lanthanum MOF polymorphs: insights into kinetically and thermodynamically controlled phases. Inorg. Chem. **48**, 4707–4713 (2009)
39. Dikhtiarenko, A., Serra-Crespo, P., Castellanos, S., Pustovarenko, A., Mendoza-Meroño, R., Garcia-Granda, S., Gascon, J.: Temperature-dependent supramolecular isomerism of lutetium-aminoterephthalate metal-organic frameworks: synthesis, crystallography, and physical properties. Cryst. Growth. Des. **16**, 5636–5645 (2016)
40. Martí-Rujas, J., Kawano, M.: Kinetic products in coordination networks: ab initio X-ray powder diffraction analysis. Acc. Chem. Res. **46**, 493–505 (2013)
41. Kitagawa, H., Ohtsu, H., Kawano, M.: Kinetic assembly of a thermally stable porous coordination network based on labile CuI units and the visualization of I_2 sorption. Angew. Chem. Int. Ed. **52**, 12395–12399 (2013)
42. Kawano, M., Haneda, T., Hashizume, D., Izumi, F., Fujita, M.: A selective instant synthesis of a coordination network and its ab initio powder structure determination. Angew. Chem. Int. Ed. **47**, 1269–1271 (2008)
43. Biradha, K., Fujita, M.: A springlike 3D-coordination network that shrinks or swells in a crystal-to-crystal manner upon guest removal or readsorption. Angew. Chem. Int. Ed. **41**, 3392–3395 (2002)
44. Ohara, K., Martí-Rujas, J., Haneda, T., Kawano, M., Hashizume, D., Izumi, F., Fujita, M.: Formation of a thermally stable, porous coordination network via a crystalline-to-amorphous-to-crystalline phase transition. J. Am. Chem. Soc. **131**, 3860–3861 (2009)
45. Martí-Rujas, J., Islam, N., Hashizume, D., Izumi, F., Fujita, M., Kawano, M.: Dramatic structural rearrangements in porous coordination networks. J. Am. Chem. Soc. **133**, 5853–5860 (2011)
46. Ohtsu, H., Bennett, T.D., Kojima, T., Keen, D.A., Niwa, Y., Kawano, M.: Amorphous–amorphous transition in a porous coordination polymer. Chem. Commun. **53**, 7060–7063 (2017)
47. Bennett, T.D., Goodwin, A.L., Dove, M.T., Keen, D.A., Tucker, M.G., Barney, E.R., Soper, A.K., Bithell, E.G., Tan, J.C., Cheetham, A.K.: Structure and properties of an amorphous metal-organic framework. Phys. Rev. Lett. **104**, 115503 (2010)
48. Bennett, T.D., Cheetham, A.K.: Amorphous metal-organic frameworks. Acc. Chem. Res. **47**, 1555–1562 (2014)
49. Bennett, T.D., Tan, J.C., Yue, Y., Baxter, E., Ducati, C., Terrill, N.J., Yeung, H.H.M., Zhou, Z., Chen, W., Henke, S., Cheetham, A.K., Greaves, G.N.: Hybrid glasses from strong and fragile metal-organic framework liquids. Nat. Commun. **6**, 8079 (2015)
50. Martí-Rujas, J., Matsushita, Y., Izumi, F., Fujita, M., Kawano, M.: Solid–liquid interface synthesis of microcrystalline porous coordination networks. Chem. Commun. **46**, 6515–6517 (2010)
51. Cavallo, G., Metrangolo, P., Milani, R., Pilati, T., Priimagi, A., Resnati, G., Terraneo, G.: The halogen bond. Chem. Rev. **116**, 2478–2601 (2016)
52. Resnati, G., Boldyreva, E., Bombicz, P., Kawano, M.: Supramolecular interactions in the solid state. IUCrJ **2**, 675–690 (2015)
53. Takaoka, K., Kawano, M., Ozeki, T., Fujita, M.: Crystallographic observation of an olefin photodimerization reaction that takes place via thermal molecular tumbling within a self-assembled host. Chem. Commun. **15**, 1625–1627 (2006)
54. Ohmori, O., Kawano, M., Fujita, M.: A two-in-one crystal: uptake of two different guests into two distinct channels of a biporous coordination network. Angew. Chem. Int. Ed. **44**, 1962–1964 (2005)

55. Ohmori, O., Kawano, M., Fujita, M.: Construction of biporous coordination networks via π−π interaction. CrystEngComm **7**, 255–259 (2005)
56. Kawano, M., Kawamichi, T., Haneda, T., Kojima, T., Fujita, M.: The modular synthesis of functional porous coordination networks. J. Am. Chem. Soc. **129**, 15418–15419 (2007)
57. Kawamichi, T., Kodama, T., Kawano, M., Fujita, M.: Single-crystalline molecular flasks: chemical transformation with bulky reagents in the pores of porous coordination networks. Angew. Chem. Int. Ed. **47**, 8030–8032 (2008)
58. Haneda, T., Kawano, M., Kawamichi, T., Fujita, M.: Direct observation of the labile imine formation through single-crystal-to-single-crystal reactions in the pores of a porous coordination network. J. Am. Chem. Soc. **130**, 1578–1579 (2008)
59. Kawamichi, T., Inokuma, Y., Kawano, M., Fujita, M.: Regioselecitive Huisgen cycloaddition within porous coordination networks. Angew. Chem. Int. Ed. **49**, 2375–2377 (2010)
60. Kawamichi, T., Haneda, T., Kawano, M., Fujita, M.: X-ray observation of a transient hemiaminal trapped in a porous network. Nature **461**, 633–635 (2009)
61. Inokuma, Y., Kawano, M., Fujita, M.: Crystalline molecular flasks. Nat. Chem. **3**, 349–358 (2011)
62. Ohtsu, H., Choi, W., Islam, N., Matsushita, Y., Kawano, M.: Selective trapping of labile S_3 in a porous coordination network and the direct X-ray observation. J. Am. Chem. Soc. **135**, 11449–11452 (2013)
63. Steudel, R., Eckert, B.: Solid sulfur allotropes. Top. Curr. Chem. **230**, 1–79 (2003)
64. Steudel, R., Steudel, Y., Wong, M.W.: Speciation and thermodynamics of sulfur vapor. Top. Curr. Chem. **230**, 117–134 (2003)
65. Meyer, B.: Elemental sulfur. Chem. Rev. **76**, 367–388 (1976)
66. McCarthy, M.C., Thorwirth, S., Gottlieb, C.A., Thaddeus, P., Gupta, H., Stanton, J.F.: Rotational spectroscopy and equilibrium structures of S_3 and S_4. J. Chem. Phys. **123**, 054326 (2005)
67. Ichikawa, M., Kimura, T., Fukuoka, A.: Stud. Surf. Sci. Catal. **60**, 335–342 (1991)
68. Maleki, B., Salehabadi, H.: Ammonium chloride; as a mild and efficient catalyst for the synthesis of some 2-arylbenzothiazoles and bisbenzothiazole derivatives. Eur. J. Chem. **4**, 377–380 (2010)
69. Choi, W., Ohtsu, H., Matsushita, Y., Kawano, M.: Safe P_4 reagent in a reusable porous coordination network. Dalton Trans. **45**, 6357–6360 (2016)
70. Ohtsu, H., Kawano, M.: Br_2 induced oxidative pore modification of a porous coordination network. Dalton Trans. **45**, 489–493 (2016)
71. Lang, J.P., Xu, Q.F., Yuan, R.X., Abrahams, B.F.: $\{[WS_4Cu_4(4,4'\text{-bpy})_4][WS_4Cu_4I_4(4,4'\text{-bpy})_2]\}_\infty$—an unusual 3D porous coordination polymer formed from the preformed cluster $[Et_4N]_4[WS_4Cu_4I_6]$. Angew. Chem. Int. Ed. **43**, 4741–4745 (2004)
72. Holzer, W., Murphy, W.F., Bernstein, H.J.: Resonance Raman effect and resonance fluorescence in halogen gases. J. Chem. Phys. **52**, 399–407 (1970)
73. Congeduti, A., Nardone, M., Postorino, P.: Polarized Raman spectra of a single crystal of iodine. Chem. Phys. **256**, 117–123 (2000)
74. Bondi, A.: van der Waals volumes and radii. J. Phys. Chem. **68**, 441–451 (1964)
75. El-Sheshtawy, H.S., Bassil, B.S., Assaf, K.I., Kortz, U., Nau, W.M.: Halogen bonding inside a molecular container. J. Am. Chem. Soc. **134**, 19935–19941 (2012)
76. Ohtsu, H., Kawano, M.: Kinetic assembly of coordination networks. Chem. Commun. **53**, 8818–8829 (2017)
77. Hathaway, B.J.: In: Wilkinson, G., Gillard, R.D., McCleverty, J.A. (eds.) Comprehensive Coordination Chemistry, vol. 5, pp. 533–774. Pergamon, Oxford (1987)
78. Ohara, K., Yamaguchi, K.: Cold-spray ionization mass spectrometric detection of a coordination oligomer. Anal. Sci. **28**, 635–637 (2012)
79. Allcock, H.R., Siegel, L.A.: Phosphonitrilic compounds. III. Molecular inclusion compounds of tris(o-phenylenedioxy)phosphonitrile trimer. J. Am. Chem. Soc. **86**, 5140–5144 (1964)

80. Hertzsch, T., Budde, F., Weber, E., Hulliger, J.: Supramolecular-wire confinement of I_2 molecules in channels of the organic zeolite tris(*o*-phenylenedioxy)cyclotriphosphazenephonitrile trimer. Angew. Chem. Int. Ed. **41**, 2281–2284 (2002)
81. Kitagawa, H., Ohtsu, H., Cruz-Cabeza, A.J., Kawano, M.: Isolation and evolution of labile sulphur allotropes via kinetic encapsulation in interactive porous networks. IUCrJ **3**, 232–236 (2016)
82. Flemming, B., Wolczanski, P.T., Hoffmann, R.: Transition metal complexes of cyclic and open ozone and thiozone. J. Am. Chem. Soc. **127**, 1278–1285 (2005)
83. Mück, L.A., Lattanzi, V., Throwirth, S., McCarthy, M.C., Gauss, J.: Cyclic SiS_2: a new perspective on the walsh rules. Angew. Chem. Int. Ed. **51**, 3695–3698 (2012)